Online Sensorless Temperature Estimation of Lithium-Ion Batteries Through Electro-Thermal Coupling

Zheng, Yusheng; Che, Yunhong; Hu, Xiaosong; Sui, Xin; Teodorescu, Remus

Published in:
IEEE/ASME Transactions on Mechatronics

DOI (link to publication from Publisher):
10.1109/TMECH.2024.3367291

Publication date:
2024

Document Version
Accepted author manuscript, peer reviewed version

Online Sensorless Temperature Estimation of Lithium-ion Batteries Through Electro-thermal Coupling

Yusheng Zheng, *Graduate Student Member IEEE*, Yunhong Che, *Graduate Student Member IEEE*, Xiaosong Hu, *Fellow, IEEE*, Xin Sui, *Member, IEEE*, Remus Teodorescu, *Fellow, IEEE*

***Abstract*—Owing to the non-negligible impacts of temperature on the safety, performance, and lifespan of lithium-ion batteries (LIBs), it is essential to regulate battery temperature to an optimal range. Temperature monitoring plays a fundamental role in battery thermal management, yet it is still challenged by limited onboard temperature sensors, particularly in large-scale battery applications. As such, developing sensorless temperature estimation is of paramount importance to acquiring the temperature information of each cell in a battery system. This paper proposes an estimation approach to obtain the cell temperature by taking advantage of the electro-thermal coupling effect of batteries. An electro-thermal coupled model, which captures the interactions between the electrical and the thermal dynamics, is established, parameterized, and experimentally validated. A closed-loop observer is then designed based on this coupled model and the extended Kalman filter (EKF) to estimate the battery temperature by merely using the voltage measurement as feedback. The electro-thermal coupling effect enables the full observability of batteries' internal states from their voltage, and contributes to an accurate and robust temperature estimation. The capability of the proposed estimation method has been demonstrated via experiments, with RMSE less than 0.7 ℃ in various scenarios.**

***Index Terms*—Lithium-ion batteries, temperature estimation, thermal management, electro-thermal model, Kalman filter.**

I. Introduction

ELECTRIFICATION is one of the promising countermeasures to the ever-rising energy demand and greenhouse gas emissions [1]. In this context, LIBs have been widely deployed to many large-scale applications such as electrified transportation as well as grid energy storage systems [2], [3]. The battery systems in these applications require careful management to ensure their safe, efficient, and reliable operations. However, the negative impacts of temperature on LIBs cannot be ignored. For instance, high temperatures not only pose great threats to battery safety with the risk of thermal runaway [4], but also accelerate battery degradation by activating side reactions [5]. Low temperatures, on the other hand, cause sluggish internal electrochemistry and undermine the energy/power capabilities of LIBs [6].

To mitigate those adverse temperature effects, batteries must be thermally managed to an optimal temperature range through the thermal management system, where effective monitoring of battery temperature becomes a fundamental task. Nevertheless, out of cost and hardware complexity considerations, allocating a temperature sensor to each cell has not been satisfied in many battery systems, particularly in a system consisting of hundreds or even thousands of cells, with an average sensor-to-cell ratio of about 1/10 [7]. As a result, the amount of temperature information that can be obtained via direct sensor measurement in a battery system is extremely insufficient [8]. Such deficiency in battery temperature information brings great challenges to battery management. Possibilities exist when temperature abnormality occurs in the cell without the attached temperature sensor, while such faults can hardly be detected in time by the nearby onboard temperature sensors, which increases the safety risks of the entire battery system. Hence, it is of paramount importance to develop sensorless temperature estimation methods to monitor the state of temperature (SOT) of each cell so as to extract more temperature information about the battery system.

Existing literature has reported several sensorless SOT estimation methods with the use of electrochemical impedance, thermal models, and data-driven methods. The electrochemical impedance of the LIB at a certain frequency region can exhibit high sensitivity to temperature but low sensitivity to state of charge (SOC) [9]–[11]. By measuring such impedance online, battery temperature can be estimated via an impedance-temperature relationship which is calibrated in advance. However, the requirement of additional hardware for excitation as well as the need for relaxation before impedance measurement limit the real-time implementation of impedance-based methods in conventional battery systems [8], [12]. Other studies tried to use direct current resistance (DCR) instead of impedance to estimate battery temperature by taking

This work was partially supported by the Villum Foundation for Smart Battery project (No. 222860), and the National Natural Science Foundation of China (No. 52111530194) (*Corresponding author: Yunhong Che*).

Yusheng Zheng, Yunhong Che, Xin Sui, Remus Teodorescu are with the Department of Energy, Aalborg University, Aalborg 9220, Denmark (e-mail: yzhe@energy.aau.dk; ych@energy.aau.dk; xin@energy.aau.dk; ret@energy.aau.dk)

Xiaosong Hu is with the College of Mechanical and Vehicle Engineering, Chongqing University, Chongqing 400044, China (e-mail: xiaosonghu@ieee.org).

advantage of the load changes as an excitation [13], [14], but it is difficult to guarantee the same excitation during dynamic operations for DCR acquisition. In recent years, data-driven methods have shown great success in battery state estimations thanks to the nonlinear mapping capabilities of many machine learning (ML) algorithms [15]–[18]. When it comes to SOT estimations, although existing ML techniques can provide flexible solutions with high accuracy and do not need domain knowledge [19], [20], it is time-consuming and sometimes technically challenging to collect sufficient high-quality data used for the training process. Most importantly, the generalization capability is always a common concern for many ML-based estimations and the trained ML algorithm may fail when there is no prior information about battery temperature in the input [21], [22].

To date, thermal model-based estimation is still the most prevalent method to achieve SOT estimations with satisfactory accuracy and robustness. Thermal models built upon first principles allow insights into thermal dynamics such as heat generation, heat accumulation, and heat dissipation [23]. To facilitate online applications, many control-oriented thermal models have been developed to improve computational efficiency [24]–[26]. However, merely relying on thermal models to estimate battery SOT in an open-loop manner makes the estimation susceptible to model uncertainties and inaccurate initializations [7]. Moreover, such estimations are subjected to slow convergence speed due to the large time constant of thermal dynamics [27]. To this end, closed-loop observers need to be developed to correct estimations according to the feedback of measurement signals and promote the convergence speed of the estimation. For sensorless SOT estimations, it is impossible to obtain temperature information (e.g., surface temperature) as feedback in the absence of the temperature sensor, and therefore the feedback must be based on other signals. Sajid et al. [28] and Elsergany et al. [29] developed closed-loop observers based on empirical battery models and EKF, using measured voltage as the feedback. Compared to empirical models, electro-thermal coupled models, which better describe the electrical and thermal dynamics of LIBs with high generalization capability, can also be used to design high-performance observers [30]. Apart from the voltage signal, the measured impedance and the identified internal resistance have been reported to be feedback signals during sensorless SOT estimation [27], [31], [32].

The use of battery voltage as feedback in SOT observers brings challenges to estimations since the battery voltage is affected by its temperature indirectly. In addition, the observability of battery temperature has not been examined thoroughly in the existing literature with a non-temperature signal as feedback. To address these issues, this paper leverages the electro-thermal coupling effect to develop a closed-loop observer to estimate battery temperature merely based on its voltage. An electro-thermal coupled model is developed at first to capture both the electrical and the thermal behaviors of the battery accurately. The interaction between electrical and thermal dynamics enables the battery voltage response to be affected by its temperature. Then a closed-loop observer is designed based on this two-way electro-thermal coupling effect to estimate the battery temperature using the measurable voltage signal as the feedback to correct the state estimates. Moreover, the observability of all the internal states is examined and full observability can be guaranteed in the proposed observer, which addresses the system observability issue brought by limited measured signals.

The remainder of this paper is organized as follows. Section II describes the electro-thermal coupled model. Section III introduces setup and experiments for data acquisition. Section IV elucidates the parameterization of the electro-thermal coupled model. The proposed sensorless SOT estimation method is presented in Section V, followed by the estimation results in Section VI, and the main conclusion in Section VII.

II. Electro-Thermal Coupled Model

Interactions between the battery's electrical and thermal dynamics exist during battery operations. That is, the electrical properties, indicated by the internal resistance and voltage response, affect the heat generation of the battery. Meanwhile, the battery temperature has an impact on its internal resistance, and further changes the voltage response. Therefore, both the dynamics, as well as their interactions, should be considered during modeling. To characterize such interactions, an electro-thermal coupled model, which consists of a first-order equivalent circuit model (ECM) and a lumped-mass thermal model, is established.

A. Electrical Model

ECMs exhibit an excellent trade-off between model simplicity and fidelity when characterizing the electrical behavior of batteries. A typical ECM can be illustrated in Fig. 1, where simple electrical components such as open circuit voltage (OCV), resistors, and capacitors can be combined in a specific way to mimic the dynamic voltage response of the battery. An ECM typically consists of an OCV, an ohmic resistance (R_0), and a number of RC pairs (R_i and C_i) connected in series. Adding more RC pairs in the ECM can increase the model accuracy while the model complexity and parameterization difficulty will be increased. Therefore, ECM with only one RC pair is adopted in this article.

The governing equations of the first-order ECM can be expressed as,

$$\frac{dV_1(t)}{dt} = -\frac{1}{R_1C_1}V_1(t) + \frac{1}{C_1}I(t) \tag{1}$$

$$V_t(t) = V_{oc}(SOC) + V_1(t) + I(t)R_0 \tag{2}$$

where I is the applied current (positive for charge and negative for discharge), V_1 is the polarization voltage, V_t is the terminal voltage, V_{oc} is battery OCV which is a function of SOC. The SOC can be calculated through coulomb counting as,

$$\frac{dSOC(t)}{dt} = \frac{I(t)}{3600C_n} \tag{3}$$

where C_n denotes the nominal capacity of the battery.

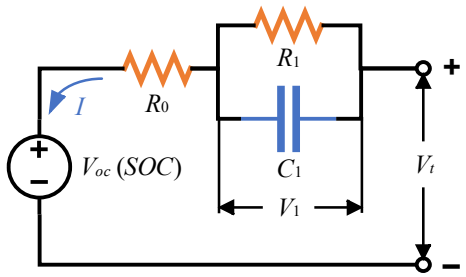

Fig. 1. Schematic of first-order ECM.

TABLE I
SPECIFICATION OF THE TESTED CELL

Cathode	NMC
Anode	Graphite
Nominal voltage	3.66 V
Nominal capacity	50 Ah
Upper cut-off voltage	4.3 V
Lower cut-off voltage	2.75 V
Battery mass	865 g
Battery surface area	4.364×10^{-2} m^2

It should be noted that the electrical parameters such as R_0, R_1, and C_1, which represent the internal electrochemistry of the battery, are dependent on both battery temperature and SOC.

The discrete-time model of the first-order ECM can be derived by applying zero-order holding (ZOH) and expressed as [33],

$$\begin{cases} SOC_{k+1} = SOC_k + \dfrac{I_k \Delta t}{3600 C_n} \\ V_{1,k+1} = V_{1,k} e^{-\frac{\Delta t}{R_1 C_1}} + I_k R_1 \left(1 - e^{-\frac{\Delta t}{R_1 C_1}}\right) \\ V_{t,k} = V_{oc}\left(SOC_k\right) + V_{1,k} + I_k R_0 \end{cases} \tag{4}$$

where Δt is the sampling interval.

B. Thermal Model

In order to characterize the battery's thermal behavior, heat generation, heat accumulation, and heat dissipation should be modeled properly. Among various control-oriented thermal models, the lumped-mass thermal model is the most computationally efficient one, which regards the battery cell as a particle and uses its bulk temperature to represent the temperature status [24]. In this way, the governing equation for thermal dynamics can be expressed as,

$$\frac{dT(t)}{dt} = -\frac{hA}{mC_p} T(t) + \frac{1}{mC_p} Q(t) + \frac{hA}{mC_p} T_f(t) \tag{5}$$

in which T is the time-varying bulk temperature, h is the equivalent convective heat transfer coefficient, A is the cell surface area, m is the cell mass, C_p is the specific heat capacity, Q is the heat generation rate, and T_f is the temperature of the heat transfer fluid.

The heat generation inside the battery consists of several heat sources, and a simplified model derived by Bernardi et al. [34] can be used to calculate heat generation, which is given by,

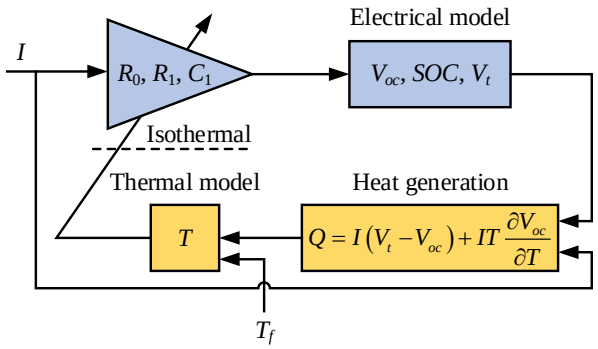

Fig. 2. Two-way coupling relationship between the electrical and the thermal models.

$$Q(t) = I(t)\left[V_t(t) - V_{oc}\left(SOC\right)\right] + I(t)T(t)\frac{\partial V_{oc}}{\partial T}\left(SOC\right) \tag{6}$$

in which the first term on the right-hand side denotes the irreversible heat of the cell and the second term represents the reversible heat due to entropy change, where $\partial V_{oc}/\partial T$ is the entropic heat coefficient and is a function of battery SOC. According to the ECM, the voltage drop inside the cell, which contributes to the irreversible heat, is caused by the ohmic resistance and the RC pair. Therefore, Eq. (6) can be further derived as,

$$Q(t) = I(t)^2 R_0 + I(t)V_1(t) + I(t)T(t)\frac{\partial V_{oc}}{\partial T}\left(SOC\right) \tag{7}$$

The discrete-time thermal model can also be derived by applying the ZOH and is expressed as [24],

$$Q_k = I_k^2 R_0 + I_k V_{1,k} + I_k T_k \frac{\partial V_{oc}}{\partial T}\left(SOC_k\right) \tag{8}$$

$$T_{k+1} = T_k e^{-\frac{hA}{mC_p}\Delta t} + \left(1 - e^{-\frac{hA}{mC_p}\Delta t}\right)\left(\frac{Q_k}{hA} + T_{f,k}\right) \tag{9}$$

C. Electro-thermal Coupling

Since the electrical behavior and thermal behavior of LIBs have interactions, a two-way coupling relationship proposed by Lin et al. can be used to capture such interactions [35], as illustrated in Fig. 2. The terminal voltage and the SOC of the battery will be calculated by the electrical model at first according to the applied current I and the electrical parameters R_0, R_1, and C_1. Then heat generation can be obtained based on the difference between the calculated terminal voltage and OCV, as well as the current I. This heat generation is fed into the thermal model to calculate the bulk temperature. The calculated bulk temperature can then be used to determine the value of electrical parameters in the electrical model. In this way, with the electrical parameters changed by the battery temperature, the impact of the thermal behavior on battery voltage can be characterized.

According to the two-way coupling relationship, the change in battery temperature will ultimately influence the way of its voltage response, though in an indirect manner. As such, it is possible to infer battery temperature merely based on how its voltage responds to the applied current if both the electrical and thermal dynamics are known in advance. In light of this, the

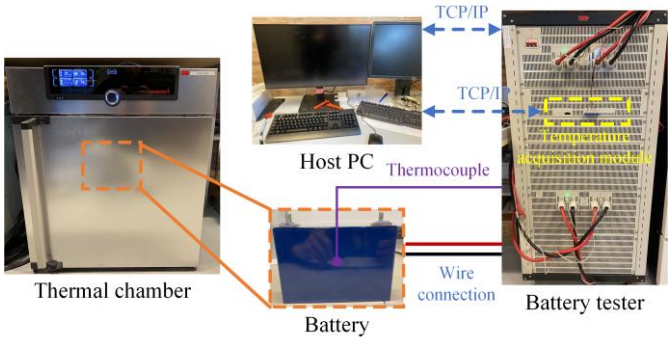

Fig. 3. Experimental setup for parameterization and validation.

two-way coupling effect can be leveraged to develop a closed-loop sensorless SOT observer in this article.

III. Experimental

Experiments were conducted with a 50-Ah prismatic cell (CALB Model L148N50B) to parameterize the electro-thermal model and generate the validation data. The specification of the cell is shown in Table I and the experimental setup used in this study is illustrated in Fig. 3. The test platform includes a Neware BTS-8000 battery tester, a thermal chamber, a host computer, and a Neware temperature acquisition module.

The tested cell was placed in a thermal chamber where the ambient temperature was adjustable. The coolant in this study is air so that T_f in the thermal model refers to the ambient temperature. In real-world applications, different coolant (e.g., liquid) might be used in the thermal management system and the temperature of the coolant temperature can usually be measured. As for the measurement of the cell temperature, it is technically difficult to measure its bulk temperature, which brings challenges to model validation. Considering this, the tested cell is thermally insulated with the method in ref. [31], [36] to reduce the internal thermal gradient of the cell. In this way, the temperature measured by a T-type thermocouple at the center of the cell surface can be regarded as the bulk temperature due to the small temperature gradient [1].

In order to parameterize the electrical model, several characterization tests were carried out, including the OCV test and hybrid pulse power characterization (HPPC) tests. During the OCV test, the cell was cycled at 1/20 C at room temperature, with a 2-h rest between the charge and discharge phase. Afterward, HPPC tests were conducted to extract other parameters of the ECM. Specifically, a discharge current of 1 C was used to adjust the battery SOC, followed by a 2-h rest and the subsequent HPPC profile. Each HPPC profile consists of a 10-s discharge pulse, a 40-s rest period, a 10-s charge pulse, and a 3-min rest period. The current during the charge and discharge pulse was also 1C. The HPPC tests were conducted at 0.9, 0.7, 0.5, 0.3, and 0.1 SOCs, which were repeated at different ambient temperatures (i.e., 25 ℃, 30 ℃, 35 ℃, 40 ℃, 45 ℃, and 50 ℃).

[1] Note that this thermal boundary condition was created deliberately to help the validation of the proposed method. Under normal operations where thermal gradient inside the cell is larger, the proposed method can be used to estimate the volume-averaged temperature after re-calibrating the convective heat transfer coefficient h.

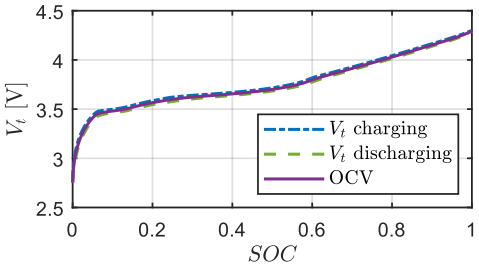

Fig. 4. Terminal voltage vs. SOC when the cell is cycled under 1/20 C.

Some thermal parameters, including the specific heat capacity C_p, the convective heat transfer coefficient h, and the entropic heat coefficient $\partial V_{oc}/\partial T$, need to be determined through experiments. The entropic heat coefficient can be determined through HPPC tests, while other parameters can be identified under dynamic tests where the current profiles were derived from real-world driving cycles. In this study, the federal urban driving schedule (FUDS), worldwide harmonized light vehicles test procedure (WLTP), Artemis driving cycles, and federal test procedure (FTP)-75 were conducted, with some cycles used for thermal model parameterization, and the others for the validation of the electro-thermal coupled model and the proposed SOT observer. Each dynamic test started from the fully charged state after 1C constant current-constant voltage (CC-CV) charging and ended when the terminal voltage reached the lower cut-off voltage.

IV. Model Parameterization and Validation

Parameterization is of great importance to the fidelity of the coupled model and further impacts the estimation accuracy. To reduce the parameterization difficulty, the electrical and thermal sub-models should be decoupled and parameterized individually [35].

A. Parameterization of the Electrical Model

When parameterizing the electrical model, battery temperature should remain constant to avoid the change of electrical parameters with temperatures. During the OCV test, the battery temperature was maintained constant at room temperature and the cell was cycled at a close-to-equilibrium state under a small current. Therefore, the terminal voltage has a small deviation from the OCV. The voltage during charging and discharging were quite close to each other, as shown in Fig. 4, and their average was treated as the battery OCV.

Then the current and voltage data in HPPC tests are used to extract the parameters of the ECM. Due to the short excitation period and low current rate, battery SOC and temperature remain basically unchanged so that ECM parameters can be treated as constants during each HPPC profile. Then the identification of the ECM parameters becomes an optimization problem where the optimal parameters are determined by minimizing the Euclidean distance between the ECM output and the measured voltage during an HPPC profile, as given by

$$\boldsymbol{\theta}_{el}^{*} = \arg\min_{\boldsymbol{\theta}_{el}} \sum_{k=1}^{N} \left(\hat{V}_{t,k} - V_{t,k} \right)^2 \tag{10}$$

where $\boldsymbol{\theta}_{el}$ is the optimization variable and in this case $\boldsymbol{\theta}_{el} = [R_0, R_1, C_1]^T$, N is the length of the voltage sequence of a

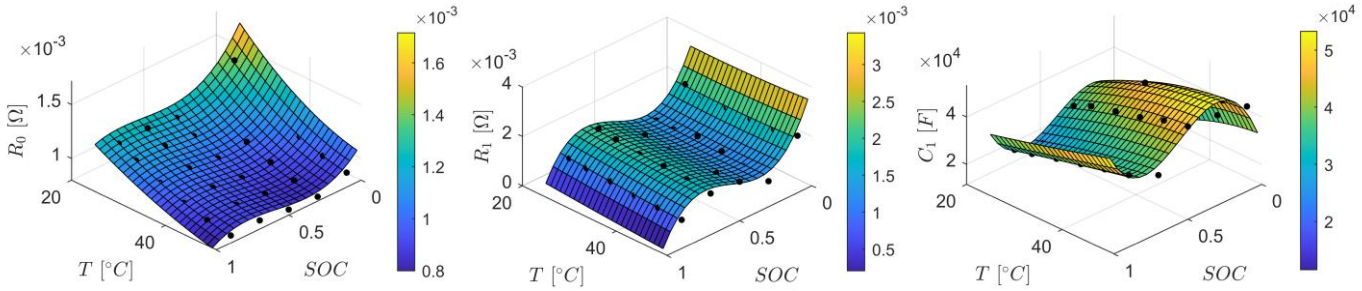

Fig. 5. Dependency of ECM parameters on SOC and temperature. The black dots are the identified value at the certain SOC and temperatures.

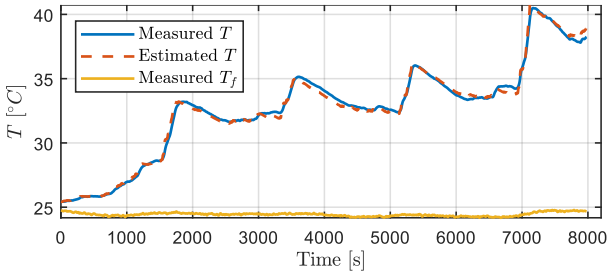

Fig. 6. Comparison between the measured temperature and estimated temperature during model parameterization.

HPPC test, $\hat{V}_{t,k}$ and $V_{t,k}$ denote the estimated voltage by ECM and the measured voltage, respectively. Particle swarm optimization (PSO) is applied to find the optimal ECM parameters because of its gradient-free search pattern, which increases the possibility of finding the global optimum. In this study, the number of particles is set to 30 and the maximum number is 600.

The identified ECM parameters at different SOCs and temperatures can be illustrated as the black dots in Fig. 5. Since these parameters vary with both SOC and temperature, polynomials models in Eq. (11) are built to describe such dependencies, where $a_i, b_i, c_i \left(i = 0,1,\ldots,8\right)$ are fitting coefficients. The fitting results can also be illustrated in Fig. 5, where the R^2 of fitting are 0.9962, 0.9449, and 0.9418, respectively.

$$\begin{cases} R_0\left(SOC,T\right) = a_0 + a_1 SOC + a_2 T + a_3 SOC^2 + a_4 SOC \cdot T + a_5 T^2 \\ \qquad + a_6 SOC^3 + a_7 SOC^2 \cdot T + a_8 SOC \cdot T^2 \\ R_1\left(SOC,T\right) = b_0 + b_1 SOC + b_2 T + b_3 SOC^2 + b_4 SOC \cdot T + b_5 T^2 \\ \qquad + b_6 SOC^3 + b_7 SOC^2 \cdot T + b_8 SOC \cdot T^2 \\ C_1\left(SOC,T\right) = c_0 + c_1 SOC + c_2 T + c_3 SOC^2 + c_4 SOC \cdot T + c_5 T^2 \\ \qquad + c_6 SOC^3 + c_7 SOC^2 \cdot T + c_8 SOC \cdot T^2 \end{cases} \tag{11}$$

B. Parameterization of the Thermal Model

To parameterize the thermal model, the experimental data from the HPPC tests and WLTP profile are used in this study. $\partial V_{oc}/\partial T$ can be calculated by linearly fitting the 2-h relaxation voltage and temperatures at certain SOC in HPPC tests, and the slope of the linear fitting can be taken as the entropic heat coefficient at this SOC [37]. In this way, the value of $\partial V_{oc}/\partial T$ at 0.9, 0.7, 0.5, 0.3, and 0.1 SOCs can be obtained. Similar to the parameter identification in the electrical model, the optimal parameters of the thermal model can be determined by minimizing the Euclidean distance between the model output and the measured temperature, which can be described as,

$$\boldsymbol{\theta}_{th}^{\ *} = \arg\min_{\boldsymbol{\theta}_{th}} \sum_{k=1}^{N} \left(\hat{T}_k - T_k\right)^2 \tag{12}$$

where $\boldsymbol{\theta}_{th} = \left[C_p, h\right]^T$, $\hat{T}_k$ and T_k are the estimated and measured temperatures at the time step k, respectively. The heat generation rate, as one of the inputs to the thermal model, is calculated based on Eq. (6). PSO can also be leveraged here to find the optimal thermal parameters and the identified C_p and h are 0.8519 $J/(g{\cdot}K)$ and 6.353 $W/(m^2{\cdot}K)$, respectively.

With the identified thermal model parameters, the comparison between the thermal model output and the measured surface temperature in the parameterization profile (i.e., WLTP) can be illustrated in Fig. 6. The parameterized thermal model has good accuracy in capturing the surface temperature of the cell, with the root mean square error (RMSE) of 0.25 ℃.

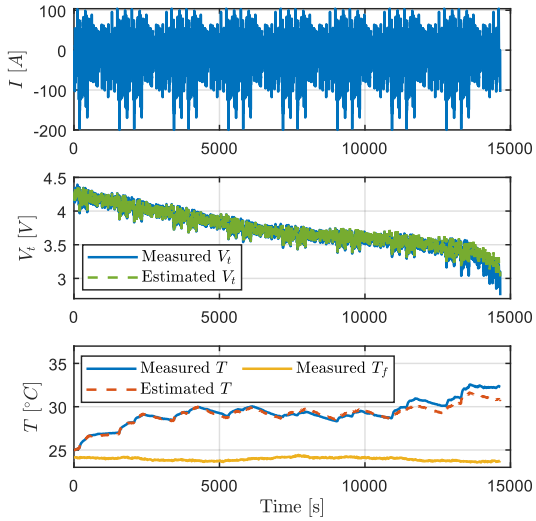

Fig. 7. Validation of the electro-thermal coupled model in terms its voltage and temperature accuracy under FTP-75 driving cycle.

C. Validation of the Coupled Model

After the parameterization, the coupled model is then validated against the FTP-75 driving profile to demonstrate its capability of capturing both the electrical and thermal dynamics of the cell. The validation results can be shown in Fig. 7. The RMSEs of the voltage estimation and temperature estimation are 25.3 mV and 0.42 ℃, respectively. It can be seen from Fig. 7 that the coupled model only has increased estimation error at a very low SOC region, while the model performance is

satisfactory in a wide SOC region. The reason for the increased estimation error at low SOC region is that the polynomials models in Eq. (11), parameterized using parameter data above 0.1 SOC, cannot capture the significant change in electrical parameters when SOC is lower than 0.1, causing increased errors for both the electrical model and the thermal model. To better capture the variation of electrical parameters, more HPPC tests can be conducted in this low SOC range to extract electrical parameters so that the model accuracy can be improved. Generally, considering other factors such as charge/discharge difference [38], load and rest difference [36], as well as rate dependence of ECM parameters [39], can also improve the model accuracy and contribute to better estimation accuracy of the observer. These factors should be carefully selected according to the battery characteristics during the modeling process so as to balance the model fidelity, complexity, and parameterization difficulty.

V. Online Sensorless Temperature Estimation

A general framework for sensorless SOT estimation in this paper can be illustrated in Fig. 8. With the measured current and ambient temperature as input, the electro-thermal model produces a voltage estimation based on the initial states. Then the estimated voltage is compared with the measured one, and the error feeds back to the electro-thermal model with a gain factor K to correct the estimations of internal states. To develop this closed-loop sensorless temperature observer, the system input, states, and output must be defined in the first place. A general discrete-time model of a nonlinear system can be applied to describe the coupled electro-thermal behavior of the battery as

$$\begin{cases} \mathbf{x}_{k+1} = f\left(\mathbf{x}_k, \mathbf{u}_k\right) + \mathbf{w}_k \\ y_k = g\left(\mathbf{x}_k, \mathbf{u}_k\right) + v_k \end{cases} \tag{13}$$

where the system input, states, and output are $\mathbf{u}_k = \left[I_k, T_{f,k}\right]^T$, $\mathbf{x}_k = \left[SOC_k, V_{1,k}, T_k\right]^T$, and $y_k = V_{t,k}$, respectively. $\mathbf{w}_k$ and v_k are the noise of the system states and measurement, with covariance matrix $\mathbf{R}_w$ and R_v, respectively. $f\left(\mathbf{x}_k, \mathbf{u}_k\right)$ and $g\left(\mathbf{x}_k, \mathbf{u}_k\right)$ are the nonlinear system state equation and output equation respectively, and can be expressed as,

$$f\left(\mathbf{x}_k, \mathbf{u}_k\right) = \begin{bmatrix} SOC_k + \dfrac{I_k \Delta t}{3600 C_n} \\ V_{1,k} e^{-\frac{\Delta t}{R_1(SOC_k,T_k)C_1(SOC_k,T_k)}} + I_k R_1 \left(1 - e^{-\frac{\Delta t}{R_1(SOC_k,T_k)C_1(SOC_k,T_k)}}\right) \\ T_k e^{-\frac{hA}{mC_p}\Delta t} + \left(1 - e^{-\frac{hA}{mC_p}\Delta t}\right)\left(\dfrac{Q_k}{hA} + T_{f,k}\right) \end{bmatrix} \tag{14}$$

$$g\left(\mathbf{x}_k, \mathbf{u}_k\right) = V_{oc}\left(SOC_k\right) + V_{1,k} + I_k R_0\left(SOC_k, T_k\right) \tag{15}$$

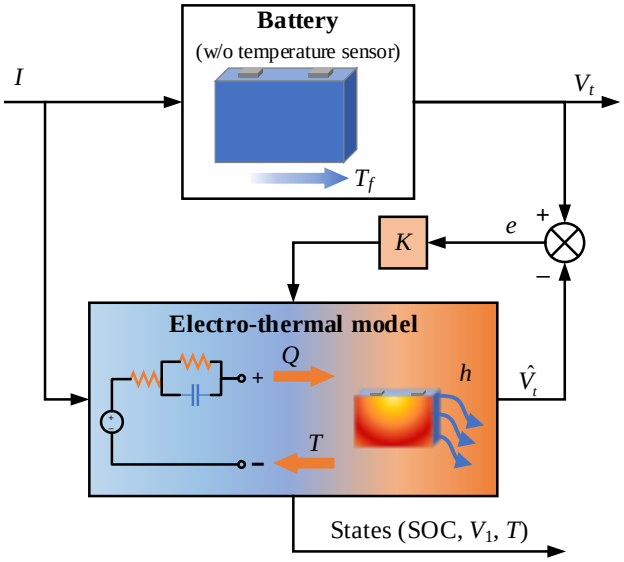

Fig. 8. Framework for sensorless SOT estimation using the measured voltage as feedback.

It should be noted from Eq. (14) and Eq. (15) that this electro-thermal coupled model is a highly nonlinear system. The terminal voltage of the cell has an implicit relationship with the battery bulk temperature. To develop the closed-loop SOT observer, EKF is leveraged in this article, which applies linear approximations to the nonlinear state and output equations, making it suitable for online applications.

Generally, EKF includes two update processes after the initialization, namely the time update process and the measurement update process. In the time update process, both the state and the error covariances will be updated as follows

$$\hat{\mathbf{x}}_k^- = f\left(\hat{\mathbf{x}}_{k-1}^+, \mathbf{u}_{k-1}\right) \tag{16}$$

$$\mathbf{P}_k^- = \mathbf{F}_{k-1}\mathbf{P}_{k-1}^+\mathbf{F}_{k-1}^T + \mathbf{R}_w \tag{17}$$

where $\hat{\mathbf{x}}_k^-$ and $\hat{\mathbf{x}}_{k-1}^+$ are the priori and posteriori estimation of the states, and $\mathbf{P}_k^-$ and $\mathbf{P}_{k-1}^+$ are the corresponding error covariances, $\mathbf{F}_{k-1}$ is the Jacobian matrix of the partial derivatives of f to $\mathbf{x}$

$$\mathbf{F}_k = \left.\frac{\partial f\left(\mathbf{x}_k, \mathbf{u}_k\right)}{\partial \mathbf{x}_k}\right|_{\mathbf{x}_k = \hat{\mathbf{x}}_k^+, \mathbf{u}_k} = \begin{bmatrix} \dfrac{\partial f_1}{\partial SOC_k} & \dfrac{\partial f_1}{\partial V_{1,k}} & \dfrac{\partial f_1}{\partial T_k} \\ \dfrac{\partial f_2}{\partial SOC_k} & \dfrac{\partial f_2}{\partial V_{1,k}} & \dfrac{\partial f_2}{\partial T_k} \\ \dfrac{\partial f_3}{\partial SOC_k} & \dfrac{\partial f_3}{\partial V_{1,k}} & \dfrac{\partial f_3}{\partial T_k} \end{bmatrix} \tag{18}$$

Elements in the Jacobian matrix are expressed in Eqs. (19)-(21). It should be noted that due to the existence of electro-thermal coupling, the ECM parameters are a function of two internal states, namely the SOC and T. Therefore, chain rules are applied when deriving the Jacobian matrix.

$$\frac{\partial f_1}{\partial SOC_k} = 1, \frac{\partial f_1}{\partial V_{1,k}} = 0, \frac{\partial f_1}{\partial T_k} = 0 \tag{19}$$

$$
\begin{cases}
\dfrac{\partial f_2}{\partial SOC_k} = V_{1,k} e^{-\frac{\Delta t}{R_1 C_1}} \left(\dfrac{1}{R_1 C_1^2} \dfrac{\partial C_1}{\partial SOC_k} + \dfrac{1}{R_1^2 C_1} \dfrac{\partial R_1}{\partial SOC_k} \right) \\
\qquad + I_k \left(1 - e^{-\frac{\Delta t}{R_1 C_1}} \right) \dfrac{\partial R_1}{\partial SOC_k} \\
\qquad - I_k R_1 e^{-\frac{\Delta t}{R_1 C_1}} \left(\dfrac{1}{R_1 C_1^2} \dfrac{\partial C_1}{\partial SOC_k} + \dfrac{1}{R_1^2 C_1} \dfrac{\partial R_1}{\partial SOC_k} \right) \\
\dfrac{\partial f_2}{\partial V_{1,k}} = e^{-\frac{\Delta t}{R_1 C_1}} \\
\dfrac{\partial f_2}{\partial T_k} = V_{1,k} e^{-\frac{\Delta t}{R_1 C_1}} \left(\dfrac{1}{R_1 C_1^2} \dfrac{\partial C_1}{\partial T_k} + \dfrac{1}{R_1^2 C_1} \dfrac{\partial R_1}{\partial T_k} \right) \\
\qquad + I_k \left(1 - e^{-\frac{\Delta t}{R_1 C_1}} \right) \dfrac{\partial R_1}{\partial T_k} \\
\qquad - I_k R_1 e^{-\frac{\Delta t}{R_1 C_1}} \left(\dfrac{1}{R_1 C_1^2} \dfrac{\partial C_1}{\partial T_k} + \dfrac{1}{R_1^2 C_1} \dfrac{\partial R_1}{\partial T_k} \right)
\end{cases}
\tag{20}
$$

$$
\begin{cases}
\dfrac{\partial f_3}{\partial SOC_k} = \dfrac{1 - e^{-\frac{hA}{mC_p}\Delta t}}{hA} \left(I_k^2 \dfrac{\partial R_0}{\partial SOC_k} + I_k T_k \dfrac{\partial \left(\partial V_{oc} / \partial T \right)}{\partial SOC_k} \right) \\
\dfrac{\partial f_3}{\partial V_{1,k}} = \dfrac{I_k \left(1 - e^{-\frac{hA}{mC_p}\Delta t} \right)}{hA} \\
\dfrac{\partial f_3}{\partial T_k} = e^{-\frac{hA}{mC_p}\Delta t} + \dfrac{1 - e^{-\frac{hA}{mC_p}\Delta t}}{hA} \left(I_k^2 \dfrac{\partial R_0}{\partial T_k} + I_k \dfrac{\partial V_{oc}}{\partial T} \left(SOC_k \right) \right)
\end{cases}
\tag{21}
$$

The measurement update process includes the calculation of the Kalman gain matrix, measurement update of the state estimation, and measurement update of the error covariance, which can be expressed as

$$\mathbf{K}_k = \mathbf{P}_{k-1}^- \mathbf{G}_k^T \left(\mathbf{G}_k \mathbf{P}_k^- \mathbf{G}_k^T + R_v \right)^{-1} \tag{22}$$

$$\hat{\mathbf{x}}_k^+ = \hat{\mathbf{x}}_k^- + \mathbf{K}_k \left(y_k - g\left(\hat{\mathbf{x}}_k^-, \mathbf{u}_k \right) \right) \tag{23}$$

$$\mathbf{P}_k^+ = \left(\mathbf{I} - \mathbf{K}_k \mathbf{G}_k \right) \mathbf{P}_k^- \tag{24}$$

where $\mathbf{K}_k$ is the Kalman gain for the states, and $\mathbf{G}_k$ is the partial derivatives of g to $\mathbf{x}$

$$
\begin{aligned}
\mathbf{G}_k &= \left. \frac{\partial g\left(\mathbf{x}_k, \mathbf{u}_k \right)}{\partial \mathbf{x}_k} \right|_{\mathbf{x}_k = \hat{\mathbf{x}}_k^-, \mathbf{u}_k} \\
&= \begin{bmatrix} \dfrac{\partial g}{\partial SOC_k} & \dfrac{\partial g}{\partial V_{1,k}} & \dfrac{\partial g}{\partial T_k} \end{bmatrix}
\end{aligned}
\tag{25}
$$

The elements in the Jacobian matrix $\mathbf{G}_k$ is calculated in Eq. (26). Similarly, since the measurement $V_{t,k}$ is not an explicit function of battery SOC and temperature, the chain rule needs to be applied again when calculating the partial derivatives of g with respect to SOC and T.

$$
\begin{cases}
\dfrac{\partial g}{\partial SOC_k} = \dfrac{\partial V_{oc}}{\partial SOC_k} + I_k \dfrac{\partial R_0}{\partial SOC_k} \\
\dfrac{\partial g}{\partial V_{1,k}} = 1 \\
\dfrac{\partial g}{\partial T_k} = I_k \dfrac{\partial R_0}{\partial T_k}
\end{cases}
\tag{26}
$$

By implementing Eqs. (16)-(17) and Eqs. (22)-(24) iteratively, the states of the electro-thermal system can be estimated.

For many nonlinear systems with limited measurement feedback, observability could be a major issue that brings challenges to tracking the real system states via the system input and output [40], [41]. In our case, since battery voltage is not an explicit function of temperature, the bulk temperature may not be estimated via terminal voltage using conventional observers [30], [42]. With the electro-thermal coupling effect, the impact of battery temperature on the terminal voltage can be characterized through ECM parameters, and this coupling effect helps guarantee the observability of the battery states. To examine the observability, the Gramian observability matrix is calculated numerically at each time step k [28], [41], i.e.,

$$\mathbf{O}_k = \left[\mathbf{G}_k, \mathbf{G}_k \mathbf{F}_k, \cdots, \mathbf{G}_k \mathbf{F}_k^{n-1} \right]^T \tag{27}$$

where $\mathbf{G}_k$ and $\mathbf{F}_k$ are calculated based on Eq. (25) and (18), respectively. The size of our system n is 3. In order to guarantee full observability, the Gramian observability matrix should have full rank (i.e., $\text{Rank}\left(\mathbf{O}\right) = n$).

VI. Results and Discussion

In this section, the proposed sensorless SOT observer will be evaluated from different aspects. We first investigate the performance of this observer under different driving profiles. Then the robustness of the observer is verified with different initial state estimates as well as measurement noises of current and voltage. Finally, this SOT observer is compared with different estimation methods, including open-loop estimations and closed-loop estimations based on empirical electro-thermal models [28].

A. SOT estimation under various driving cycles

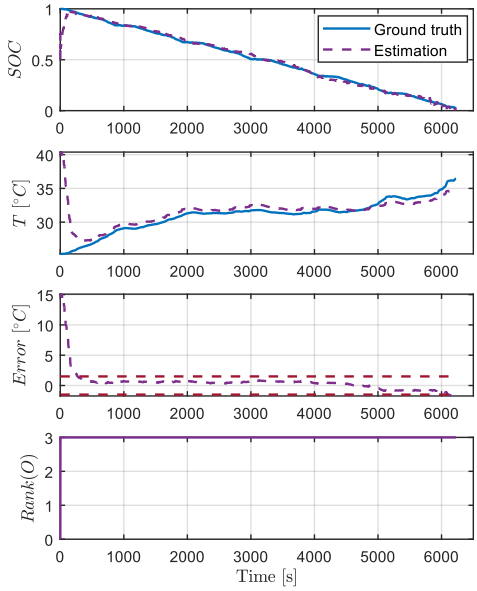

Fig. 9. Estimation results of battery SOC and temperature under Artemis cycle using the proposed observer with inaccurate initializations.

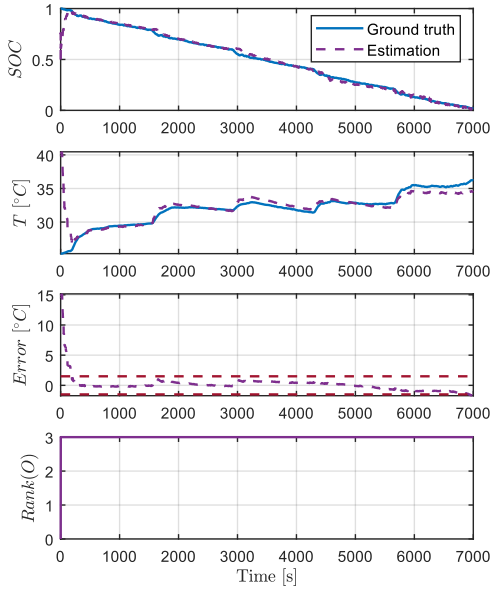

Fig. 10. Estimation results of battery SOC and temperature under FUDS cycle using the proposed observer with inaccurate initializations.

TABLE II
ESTIMATION ERROR WITH THE PROPOSED SOT OBSERVER UNDER DIFFERENT DRIVING PROFILES

Driving profiles	$0 \text{ s} < t < t_{end}$		$300 \text{ s} < t < t_{end}$	
	RMSE (℃)	MAE (℃)	RMSE (℃)	MAE (℃)
Artemis	1.94	0.91	0.67	0.62
FUDS	1.46	0.64	0.59	0.47

To validate the effectiveness of the proposed sensorless SOT observer, two driving profiles, namely the Artemis driving cycle and FUDS cycle, have been applied to evaluate its performance. One of the main advantages of the closed-loop observer is that the estimated states will converge to the real values quickly, even with inaccurate initialization of the states. The initialization of the proposed state observer is set as $\mathbf{x}_0 = [0.5, 0, 40]^T$ deliberately, i.e., the initial SOC and temperature estimates have an absolute error of 50% and 15 ℃, respectively. The covariance matrix $\mathbf{R}_w$ and R_v are set as

$$\mathbf{R}_w = diag\left(\left[3\times10^{-6}, 1\times10^{-6}, 1\times10^{-6}\right]\right), R_v = 2.5\times10^{-5}$$

The initial value of the error covariance is set as

$$\mathbf{P}_0 = diag\left(\left[1\times10^{-3}, 1\times10^{-3}, 1\right]\right)$$

The state estimation results under the Artemis driving cycle and FUDS cycle can be illustrated in Fig. 9 and Fig. 10, respectively. With the proposed observer, both the SOC and temperature estimations converge to the ground truth quickly. As for the bulk temperature, it only takes about 300 s to converge to the true value in both cycles, and the steady-state estimation errors in both cases are generally within the bounds of ±1.5 ℃, which are marked by the red dashed lines in both figures. The estimation performance of the proposed observer was evaluated by RMSE and mean absolute error (MAE), which can be summarized in Table II. After 300 s when the estimation converges, both the RMSE and MAE in these two driving cycles are lower than 0.7 ℃, demonstrating the accuracy of the proposed sensorless SOT observer.

Since observability can be an important issue affecting state estimation, the rank of the Gramian observability matrix is also calculated timely. Results in both Fig. 9 and Fig. 10 show that the rank of the observability matrix is 3 (i.e., full rank) nearly over the entire driving profile, indicating the full observability of the battery's internal states benefited from the electro-thermal coupling effect. This is also the reason for the fast convergence of the temperature estimation when merely using voltage as feedback in the designed SOT observer.

TABLE III
ESTIMATION ERROR WITH DIFFERENT TEMPERATURE INITIALIZATIONS

Temperature initializations	$0 \text{ s} < t < t_{end}$		$1000 \text{ s} < t < t_{end}$	
	RMSE (℃)	MAE (℃)	RMSE (℃)	MAE (℃)
10 ℃	2.02	1.11	0.67	0.53
15 ℃	1.50	0.88	0.60	0.47
20 ℃	1.07	0.69	0.56	0.43
30 ℃	0.85	0.55	0.57	0.45
35 ℃	1.29	0.64	0.61	0.53
40 ℃	1.94	0.91	0.67	0.61

B. Robustness Test

The robustness is another important metric to evaluate the performance of an observer. Generally, for a robust observer, the estimation of internal states should converge to the ground truth even with the presence of perturbation and noise [43]. To verify the robustness of the proposed SOT observer, different initial temperatures are provided for the observer while the initial value of SOC and V_1 remain unchanged in different cases (0.5 and 0 V respectively). The estimation results with different temperature initializations can be shown in Fig. 11(a), with the estimation errors summarized in Table III. Even with different initial temperature estimates, the proposed SOT observer can still track the real battery temperature after about 500 s. The estimation with different initializations exhibits little difference in convergence speed, but at about 1000 s all estimations have already converged to the true value. Furthermore, despite the large estimation errors at the beginning caused by inaccurate initialization, the steady-state errors for all the cases after 1000 s can be reduced to lower than 0.7 ℃. In addition, in real-world applications, larger noise exists during both current and voltage measurements compared to the lab tests, which would affect the performance of the SOT

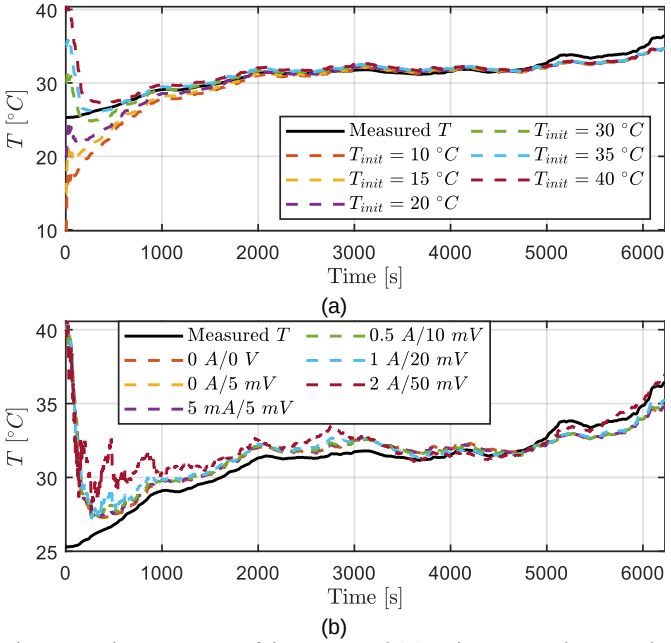

Fig. 11. Robustness test of the proposed SOT observer under Artemis driving cycle. (a) With different initial temperatures. (b) With different current and voltage measurement noise.

observer. To test the performance of the observer, zero-mean white Gaussian noises with different standard deviations have been added to the original current and voltage data, while the initialization of battery temperature, SOC and V_1 are kept as 40 °C, 0.5, and 0 V in different cases. The temperature estimation results under different noise levels are shown in Fig. 11(b). The estimation can still converge to the ground truth even with large noise in both current and voltage measurements. However, with larger noise, the convergence speed becomes slow, and the accuracy of the estimation also deteriorates. When the noise level increases beyond the studied scope in Fig. 11(b), the observer fails to work, indicating its stability within a certain noise level.

Apart from operating conditions (i.e., battery temperature and SOC), battery degradation also has an impact on the electrical parameters in the long run and therefore affects the SOT estimation. Nevertheless, the change in electrical parameters as a result of battery aging is a gradual process and such a change is not significant within dozens of cycles [44], [45]. To take the effect of aging into account, battery parameters can be updated periodically over its life cycle, where an aging compensation with offset correction can be made [14]. Moreover, online estimation of battery state of health (SOH) enables the correction of battery real capacity [46] and contributes to the quick convergence of other state estimations in the presence of SOH perturbations.

C. Comparison with different methods

There are also other sensorless temperature estimation methodologies in the existing literature, including open-loop estimations based on thermal models [47] and closed-loop estimations based on empirical models [28]. In this article, we compare the estimation performance of the proposed observer with the aforementioned two approaches under the FUDS driving cycle. The initialization of the state estimates in the

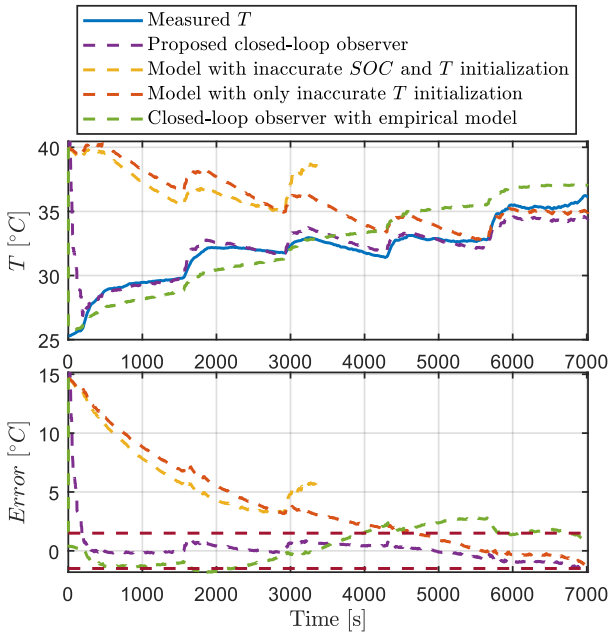

Fig. 12. Comparison between the proposed closed-loop observer and open-loop estimations under FUDS cycle and with inaccurate initializations.

TABLE IV
ERROR COMPARISON OF DIFFERENT SOT ESTIMATION METHODS

Methods	$0\ s < t < t_{end}$		$300\ s < t < t_{end}$	
	RMSE (°C)	MAE (°C)	RMSE (°C)	MAE (°C)
Proposed closed-loop observer	1.46	0.64	0.59	0.47
Open-loop estimation with inaccurate T_s	5.57	4.03	4.89	3.60
Closed-loop observer with empirical model	1.58	1.42	1.60	1.46

proposed SOT observer is $\mathbf{x}_0 = [0.5, 0, 40]^T$. As for open-loop estimations based on the electro-thermal model, two cases with inaccurate initializations have been investigated, including the case with inaccurate initial SOC and temperature estimates and the case with only inaccurate temperature estimates. As for the closed-loop estimation with the empirical battery model, an electro-thermal model is first fitted with the WLTP data using the linear model provided in [28]. The obtained relationship is expressed as

$$T_{k+1} = 0.99989T_k + 7.811*10^{-7} I_k^2 + 0.00280221 \quad (28)$$

$$V_{t,k} = -0.0184191T_k + 0.718752SOC_k + 0.00151681I_k + 3.992363 \quad (29)$$

The parameters of the closed-loop observer based on the empirical model, including the covariance matrix and initial state estimates, are set to be the same as the observer proposed in this work. The comparison results can be presented in Fig. 12 and Table IV. It can be seen from the results that the closed-loop estimations converge much faster than the open-loop estimations due to the correction of state estimates based on the measurement feedback. The closed-loop observer with the electro-thermal model exhibits much higher accuracy compared with the one with the empirical model, showing 63.13% reduction of RMSE in the steady state. The reason for the large estimation error with the empirical model is that the fitted model based on one condition can hardly maintain its

accuracy under other conditions due to the lack of insights into battery electrical and thermal dynamics. For open-loop estimation with inaccurate SOC and temperature initializations, the estimation stops because the calculated terminal voltage reaches the lower cut-off voltage. Even with accurate SOC initialization, it still takes a lot of time for the open-loop estimation to converge to the true value.

VII. Conclusion and Future Work

Sensorless temperature estimation plays a vital role in large-scale battery applications as it helps obtain the temperature information of many LIBs that lack attached temperature sensors in the context of limited onboard temperature sensors. This paper demonstrates the feasibility of closed-loop estimation of battery SOT merely based on the voltage feedback by taking advantage of the electro-thermal coupling effect. An electro-thermal coupled model considering the interactions between the electrical and the thermal dynamics is established, such that the change in battery temperature can ultimately be manifested by its voltage response. An EKF-based observer is then developed to estimate the battery bulk temperature by merely using the measured voltage as feedback. Validations against experiments show that the proposed observer can estimate battery temperature accurately under different driving profiles and inaccurate initializations. Furthermore, full observability of the internal states can be guaranteed, which contributes to quick convergence of the temperature estimation. Finally, the comparison with other approaches shows that the proposed sensorless SOT observer outperforms other methods in terms of accuracy and convergence speed.

Nevertheless, the proposed SOT estimation methodology is based on a single cell with passive cooling where the cooling coefficient remains constant. To extend such a methodology to real-world applications with multiple cells and active thermal management, where the inter-cell heat transfer and the change in cooling coefficient exist, a time-varying equivalent convective heat transfer coefficient needs to be adopted in future work. In this way, the net effect of heat dissipation to the ambient and the heat exchange between adjacent cells can be described by the heat dissipation term. Dual observers need to be developed to estimate the battery temperature and the time-varying heat transfer coefficient simultaneously.

References

[1] J. H. Williams *et al.*, "The Technology Path to Deep Greenhouse Gas Emissions Cuts by 2050: The Pivotal Role of Electricity," *Science (1979)*, vol. 335, no. 6064, pp. 53–59, Jan. 2012, doi: 10.1126/science.1208365.

[2] Z. P. Cano *et al.*, "Batteries and fuel cells for emerging electric vehicle markets," *Nature Energy*, vol. 3, no. 4. Nature Publishing Group, pp. 279–289, Apr. 01, 2018. doi: 10.1038/s41560-018-0108-1.

[3] C. Xu *et al.*, "Electric vehicle batteries alone could satisfy short-term grid storage demand by as early as 2030," *Nat Commun*, vol. 14, no. 1, p. 119, Jan. 2023, doi: 10.1038/s41467-022-35393-0.

[4] X. Feng, M. Ouyang, X. Liu, L. Lu, Y. Xia, and X. He, "Thermal runaway mechanism of lithium ion battery for electric vehicles: A review," *Energy Storage Materials*, vol. 10. Elsevier, pp. 246–267, Jan. 01, 2018. doi: 10.1016/j.ensm.2017.05.013.

[5] J. S. Edge *et al.*, "Lithium ion battery degradation: what you need to know," *Physical Chemistry Chemical Physics*, vol. 23, no. 14. pp. 8200–8221, 2021. doi: 10.1039/d1cp00359c.

[6] X. Hu, Y. Zheng, D. A. Howey, H. Perez, A. Foley, and M. Pecht, "Battery warm-up methodologies at subzero temperatures for automotive applications: Recent advances and perspectives," *Prog Energy Combust Sci*, vol. 77, 2020, doi: 10.1016/j.pecs.2019.100806.

[7] X. Lin, H. E. Perez, J. B. Siegel, and A. G. Stefanopoulou, "Robust estimation of battery system temperature distribution under sparse sensing and uncertainty," *IEEE Transactions on Control Systems Technology*, vol. 28, no. 3. pp. 753–765, 2020. doi: 10.1109/TCST.2019.2892019.

[8] Y. Zheng, Y. Che, X. Hu, X. Sui, D.-I. Stroe, and R. Teodorescu, "Thermal state monitoring of lithium-ion batteries: Progress, challenges, and opportunities," *Prog Energy Combust Sci*, vol. 100, p. 101120, Jan. 2024, doi: 10.1016/j.pecs.2023.101120.

[9] J. P. Schmidt, S. Arnold, A. Loges, D. Werner, T. Wetzel, and E. Ivers-Tiffée, "Measurement of the internal cell temperature via impedance: Evaluation and application of a new method," *J Power Sources*, vol. 243, pp. 110–117, 2013, doi: 10.1016/j.jpowsour.2013.06.013.

[10] R. Srinivasan, B. G. Carkhuff, M. H. Butler, and A. C. Baisden, "Instantaneous measurement of the internal temperature in lithium-ion rechargeable cells," *Electrochim Acta*, vol. 56, no. 17, pp. 6198–6204, 2011, doi: 10.1016/j.electacta.2011.03.136.

[11] H. P. G. J. Beelen, L. H. J. Raijmakers, M. C. F. Donkers, P. H. L. Notten, and H. J. Bergveld, "A comparison and accuracy analysis of impedance-based temperature estimation methods for Li-ion batteries," *Appl Energy*, vol. 175, pp. 128–140, 2016, doi: 10.1016/j.apenergy.2016.04.103.

[12] R. R. Richardson, P. T. Ireland, and D. A. Howey, "Battery internal temperature estimation by combined impedance and surface temperature measurement," *J Power Sources*, vol. 265, pp. 254–261, 2014, doi: 10.1016/j.jpowsour.2014.04.129.

[13] S. Ludwig, I. Zilberman, M. F. Horsche, T. Wohlers, and A. Jossen, "Pulse resistance based online temperature estimation for lithium-ion cells," *J Power Sources*, vol. 490, p. 229523, 2021, doi: 10.1016/j.jpowsour.2021.229523.

[14] S. Ludwig *et al.*, "Adaptive method for sensorless temperature estimation over the lifetime of lithium-ion batteries," *J Power Sources*, vol. 521, no. October 2021, p. 230864, 2022, doi: 10.1016/j.jpowsour.2021.230864.

[15] A. Tang, Y. Jiang, Q. Yu, and Z. Zhang, "A hybrid neural network model with attention mechanism for state of health estimation of lithium-ion batteries," *J Energy Storage*, vol. 68, p. 107734, Sep. 2023, doi: 10.1016/j.est.2023.107734.

[16] Y. Yang, L. Zhao, Q. Yu, S. Liu, G. Zhou, and W. Shen, "State of charge estimation for lithium-ion batteries based on cross-domain transfer learning with feedback mechanism," *J Energy Storage*, vol. 70, p. 108037, Oct. 2023, doi: 10.1016/j.est.2023.108037.

[17] R. Guo, Y. Xu, C. Hu, and W. Shen, "Self-Adaptive Neural Network-Based Fractional-Order Nonlinear Observer Design for State of Charge Estimation of Lithium-Ion Batteries," *IEEE/ASME Transactions on Mechatronics*, pp. 1–12, 2023, doi: 10.1109/TMECH.2023.3321719.

[18] K. Q. Zhou, Y. Qin, and C. Yuen, "Transfer-Learning-Based State-of-Health Estimation for Lithium-Ion Battery With Cycle Synchronization," *IEEE/ASME Transactions on Mechatronics*, vol. 28, no. 2, pp. 692–702, Apr. 2023, doi: 10.1109/TMECH.2022.3201010.

[19] M. Naguib, P. Kollmeyer, and A. Emadi, "Application of Deep Neural Networks for Lithium-Ion Battery Surface Temperature Estimation Under Driving and Fast Charge Conditions," *IEEE Transactions on Transportation Electrification*, 2022, doi: 10.1109/TTE.2022.3200225.

[20] Q. Yao, D. D. C. Lu, and G. Lei, "A Surface Temperature Estimation Method for Lithium-ion Battery Using Enhanced GRU-RNN," *IEEE Transactions on Transportation Electrification*, 2022, doi: 10.1109/TTE.2022.3197927.

[21] O. Ojo, H. Lang, Y. Kim, X. Hu, B. Mu, and X. Lin, "A Neural Network Based Method for Thermal Fault Detection in Lithium-Ion Batteries," *IEEE Transactions on Industrial Electronics*, vol. 68, no. 5, pp. 4068–4078, 2021, doi: 10.1109/TIE.2020.2984980.

[22] Y. Zheng, Y. Che, X. Hu, X. Sui, and R. Teodorescu, "Sensorless Temperature Monitoring of Lithium-ion Batteries by Integrating

Physics with Machine Learning," *IEEE Transactions on Transportation Electrification*, pp. 1–1, 2023, doi: 10.1109/TTE.2023.3294417.
[23] H. Liu, Z. Wei, W. He, and J. Zhao, "Thermal issues about Li-ion batteries and recent progress in battery thermal management systems: A review," *Energy Convers Manag*, vol. 150, no. August, pp. 304–330, 2017, doi: 10.1016/j.enconman.2017.08.016.
[24] X. Hu, W. Liu, X. Lin, and Y. Xie, "A Comparative Study of Control-Oriented Thermal Models for Cylindrical Li-Ion Batteries," *IEEE Transactions on Transportation Electrification*, vol. 5, no. 4. pp. 1237–1253, 2019. doi: 10.1109/TTE.2019.2953606.
[25] Y. Zhou, H. Deng, and H.-X. Li, "Control-Oriented Galerkin-Spectral Model for 3-D Thermal Diffusion of Pouch-Type Batteries," *IEEE Trans Industr Inform*, pp. 1–9, 2022, doi: 10.1109/TII.2022.3212279.
[26] X. Hu, W. Liu, X. Lin, Y. Xie, A. M. Foley, and L. Hu, "A Control-Oriented Electrothermal Model for Pouch-Type Electric Vehicle Batteries," *IEEE Trans Power Electron*, vol. 36, no. 5, pp. 5530–5544, May 2021, doi: 10.1109/TPEL.2020.3027561.
[27] R. R. Richardson and D. A. Howey, "Sensorless Battery Internal Temperature Estimation Using a Kalman Filter with Impedance Measurement," *IEEE Transactions on Sustainable Energy*, vol. 6, no. 4. pp. 1190–1199, 2015. doi: 10.1109/TSTE.2015.2420375.
[28] M. Sajid, A. A. Hussein, A. Wadi, and M. F. Abdel-Hafez, "An Enhanced Fusion Algorithm With Empirical Thermoelectric Models for Sensorless Temperature Estimation of Li-ion Battery Cells," *IEEE/ASME Transactions on Mechatronics*, pp. 1–11, 2023, doi: 10.1109/TMECH.2023.3235726.
[29] A. M. Elsergany, A. A. Hussein, A. Wadi, and M. F. Abdel-Hafez, "An Adaptive Autotuned Polynomial-Based Extended Kalman Filter for Sensorless Surface Temperature Estimation of Li-Ion Battery Cells," *IEEE Access*, vol. 10, pp. 14038–14048, 2022, doi: 10.1109/ACCESS.2022.3148281.
[30] H. Pang, L. Guo, L. Wu, J. Jin, F. Zhang, and K. Liu, "A novel extended Kalman filter-based battery internal and surface temperature estimation based on an improved electro-thermal model," *J Energy Storage*, vol. 41, no. June, p. 102854, 2021, doi: 10.1016/j.est.2021.102854.
[31] R. R. Richardson, S. Zhao, and D. A. Howey, "On-board monitoring of 2-D spatially-resolved temperatures in cylindrical lithium-ion batteries: Part II. State estimation via impedance-based temperature sensing," *Journal of Power Sources*, vol. 327. pp. 726–735, 2016. doi: 10.1016/j.jpowsour.2016.06.104.
[32] Y. Xie *et al.*, "An Enhanced Online Temperature Estimation for Lithium-Ion Batteries," *IEEE Transactions on Transportation Electrification*, vol. 6, no. 2, pp. 375–390, 2020, doi: 10.1109/TTE.2020.2980153.
[33] X. Hu, S. Li, and H. Peng, "A comparative study of equivalent circuit models for Li-ion batteries," *Journal of Power Sources*, vol. 198. pp. 359–367, 2012. doi: 10.1016/j.jpowsour.2011.10.013.
[34] D. Bernardi, E. Pawlikowski, and J. Newman, "A General Energy Balance for Battery Systems," *J Electrochem Soc*, vol. 132, no. 1, pp. 5–12, Jan. 1985, doi: 10.1149/1.2113792.
[35] X. Lin *et al.*, "A lumped-parameter electro-thermal model for cylindrical batteries," *Journal of Power Sources*, vol. 257. pp. 12–20, 2014. doi: 10.1016/j.jpowsour.2014.01.097.
[36] X. Hua, C. Zhang, and G. Offer, "Finding a better fit for lithium ion batteries: A simple, novel, load dependent, modified equivalent circuit model and parameterization method," *Journal of Power Sources*, vol. 484. 2021. doi: 10.1016/j.jpowsour.2020.229117.
[37] J. Du, Z. Chen, and F. Li, "Multi-Objective Optimization Discharge Method for Heating Lithium-Ion Battery at Low Temperatures," *IEEE Access*, vol. 6, pp. 44036–44049, 2018, doi: 10.1109/ACCESS.2018.2837652.
[38] W. Li, L. Liang, W. Liu, and X. Wu, "State of Charge Estimation of Lithium-Ion Batteries Using a Discrete-Time Nonlinear Observer," *IEEE Transactions on Industrial Electronics*, vol. 64, no. 11, pp. 8557–8565, Nov. 2017, doi: 10.1109/TIE.2017.2703685.
[39] W. Waag, S. Käbitz, and D. U. Sauer, "Experimental investigation of the lithium-ion battery impedance characteristic at various conditions and aging states and its influence on the application," *Appl Energy*, vol. 102, pp. 885–897, Feb. 2013, doi: 10.1016/j.apenergy.2012.09.030.
[40] S. Sattarzadeh, T. Roy, and S. Dey, "Real-Time Estimation of 2-D Temperature Distribution in Lithium-Ion Pouch Cells," *IEEE Transactions on Transportation Electrification*, vol. 7, no. 4. pp. 2249–2259, 2021. doi: 10.1109/TTE.2021.3071950.
[41] Y. Xiao, "Model-Based Virtual Thermal Sensors for Lithium-Ion Battery in EV Applications," *IEEE Transactions on Industrial Electronics*, vol. 62, no. 5, pp. 3112–3122, May 2015, doi: 10.1109/TIE.2014.2386793.
[42] Y. Liu, Z. Huang, Y. Wu, L. Yan, F. Jiang, and J. Peng, "An online hybrid estimation method for core temperature of Lithium-ion battery with model noise compensation," *Appl Energy*, vol. 327, p. 120037, Dec. 2022, doi: 10.1016/j.apenergy.2022.120037.
[43] E. Locorotondo, G. Lutzemberger, and L. Pugi, "State-of-charge estimation based on model-adaptive Kalman filters," *Proceedings of the Institution of Mechanical Engineers, Part I: Journal of Systems and Control Engineering*, vol. 235, no. 7, pp. 1272–1286, Aug. 2021, doi: 10.1177/0959651820965406.
[44] J. Guo *et al.*, "Unravelling and quantifying the aging processes of commercial $Li(Ni_{0.5}Co_{0.2}Mn_{0.3})O_2$ /graphite lithium-ion batteries under constant current cycling," *J Mater Chem A Mater*, vol. 11, no. 1, pp. 41–52, 2023, doi: 10.1039/D2TA05960F.
[45] S. Barcellona, S. Colnago, G. Dotelli, S. Latorrata, and L. Piegari, "Aging effect on the variation of Li-ion battery resistance as function of temperature and state of charge," *J Energy Storage*, vol. 50, p. 104658, Jun. 2022, doi: 10.1016/j.est.2022.104658.
[46] E. Locorotondo, L. Pugi, L. Berzi, M. Pierini, and A. Pretto, "Online State of Health Estimation of Lithium-Ion Batteries Based on Improved Ampere-Count Method," in *2018 IEEE International Conference on Environment and Electrical Engineering and 2018 IEEE Industrial and Commercial Power Systems Europe (EEEIC / I&CPS Europe)*, IEEE, Jun. 2018, pp. 1–6. doi: 10.1109/EEEIC.2018.8493825.
[47] N. Wang, A. Chen, W. Zhao, R. Zhu, and B. Duan, "An online temperature estimation for cylindrical lithium-ion batteries based on simplified distribution electrical-thermal model," *J Energy Storage*, vol. 55, Nov. 2022, doi: 10.1016/j.est.2022.105326.

Yusheng Zheng (Graduate Student Member, IEEE) received the B.E. degree in mechanical engineering and the M.S. degree in automotive engineering from Chongqing University, Chongqing, China, in 2018 and 2021, respectively. He is currently pursuing the Ph.D. degree with the Department of Energy, Aalborg University, Aalborg, Denmark, and a visiting PhD student with the Department of Mechanical Engineering at Imperial College London, London, UK.
His research interests include state estimation and prediction of lithium-ion batteries, battery thermal management, as well as battery fast charging.

Yunhong Che (Graduate Student Member, IEEE) received the B.E. and M.S. degrees in the College of Mechanical and Vehicle Engineering from Chongqing University, Chongqing, China, in 2019 and 2021, respectively. He is currently pursuing the Ph.D. degree with the Department of Energy, Aalborg University, Aalborg, Denmark. He was a visiting student scholar with the Institute of Civil Engineering at Swiss Federal Institute of Technology in Lausanne (EPFL), Lausanne, Switzerland, and the Department of Energy Science & Engineering at Stanford University, Stanford, USA, in 2023.
His research interests include battery health estimation and prediction, fault diagnostics, physics-informed machine learning in modeling and prognostics, and smart health management for energy storage systems.

Xiaosong Hu (Fellow, IEEE) received the Ph.D. degree in automotive engineering from the Beijing Institute of Technology, Beijing, China, in 2012. He did scientific research and completed the Ph.D. dissertation in Automotive Research Center at the University of Michigan, Ann Arbor, MI, USA, between 2010 and 2012.

He is currently a Professor with the Department of Mechanical and Vehicle Engineering, Chongqing University, Chongqing, China. He was a Postdoctoral Researcher with the Department of Civil and Environmental Engineering, University of California, Berkeley, CA, USA, between 2014 and 2015, as well as at the Swedish Hybrid Vehicle Center and the Department of Signals and Systems at Chalmers University of Technology, Gothenburg, Sweden, between 2012 and 2014. He was also a Visiting Postdoctoral Researcher with the Institute for Dynamic Systems and Control at Swiss Federal Institute of Technology (ETH), Zurich, Switzerland, in 2014. His research interests include modeling and control of alternative powertrains and energy storage systems.

Dr. Hu has been the recipient of numerous prestigious awards/honors, including Web of Science Highly-Cited Researcher by Clarivate Analytics, SAE Environmental Excellence in Transportation Award, IEEE ITSS Young Researcher Award, SAE Ralph Teetor Educational Award, Emerging Sustainability Leaders Award, EU Marie Currie Fellowship, ASME DSCD Energy Systems Best Paper Award, and Beijing Best Ph.D. Dissertation Award. He is an IET Fellow.

Xin Sui (Member, IEEE) received the B.Eng. degree from Northeast Electric Power University, Jilin, China, in 2015, and the M.Sc. degree from Institute of Electrical Engineering, Chinese Academy of Sciences, Beijing, China, in 2018, both in electrical engineering. In 2022, Xin received the Ph.D. degree in machine learning for battery state of health estimation from Aalborg University, Aalborg, Denmark.

She is currently a postdoctoral researcher with the Center for Research on Smart Battery (CROSBAT), AAU Energy, Aalborg University. Her research interests include battery state of health estimation, lifetime extension, feature engineering, and machine learning.

Remus Teodorescu (Fellow, IEEE) received the Dipl.Ing. degree in electrical engineering from the Politehnica University of Bucharest, Romania, in 1989, and the Ph.D. degree in power electronics from the University of Galati, Romania, in 1994.,In 1998, he joined the Power Electronics Section, AAU Energy, Aalborg University, where he currently works as a Full Professor. From 2013 to 2017, he was a Visiting Professor with the Chalmers University of Grid Converters for Photovoltaic and Wind Power Systems (Wiley-IEEE Press, 2011) and Design, Control and Application of Modular Multilevel Converters for HVDC Transmission Systems (Wiley-IEEE Press, 2016). He has coauthored over 500 IEEE journal articles and conference papers. His research interests include design and control of grid connected converters for photovoltaic and wind power systems, HVDC/FACTS based on MMC, SiC-based converters, storage systems for utility based on Li-Ion battery technology, and battery lifetime model using artificial intelligence. In 2021, he was awarded the Villum Investigator grant for the development of the Center of Research on Smart Battery at Aalborg University.